High Magnetic Field Water and Metabolite Proton T_1 and T_2 Relaxation in Rat Brain In Vivo

Robin A. de Graaf,* Peter B. Brown, Scott McIntyre, Terence W. Nixon, Kevin L. Behar, and Douglas L. Rothman

Comprehensive and quantitative measurements of T_1 and T_2 relaxation times of water, metabolites, and macromolecules in rat brain under similar experimental conditions at three high magnetic field strengths (4.0 T, 9.4 T, and 11.7 T) are presented. Water relaxation showed a highly significant increase (T_1) and decrease (T_2) with increasing field strength for all nine analyzed brain structures. Similar but less pronounced effects were observed for all metabolites. Macromolecules displayed field-independent T_2 relaxation and a strong increase of T_1 with field strength. Among other features, these data show that while spectral resolution continues to increase with field strength, the absolute signal-to-noise ratio (SNR) in T_1/T_2-based anatomical MRI quickly levels off beyond ~7 T and may actually decrease at higher magnetic fields. Magn Reson Med 56:386–394, 2006.

Key words: water T_1/T_2 relaxation; metabolite T_1/T_2 relaxation; macromolecular T_1/T_2 relaxation; high-field NMR; sensitivity; spectral resolution; brain

Magnetic fields strengths for in vivo MRI and MRS have seen a steady increase, and are currently up to 9.4 T for humans and >14 T for animals. This drive has largely been fueled by the greatly improved contrast-to-noise (CNR) ratio of functional MRI (fMRI) techniques, as well as the linear increase in signal-to-noise (SNR) ratio and spectral resolution with increasing field strength. However, although T_1 and T_2 relaxation parameters play an important role in the actual SNR and resolution, they are often ignored in discussions of high-field NMR. While the field-dependent trends for T_1 and T_2 relaxation of water have been quantitatively established for lower magnetic fields (1), no comprehensive and quantitative relaxation parameters are available for the range of high magnetic field strengths (>3 T) currently used in MR research laboratories. Some studies have reported T_1 and T_2 relaxation at one magnetic field (e.g., Refs. 2 and 3), but it is difficult to establish any quantitative trends because of large variations among laboratories. Knowledge about metabolite and macromolecule proton T_1 and T_2 relaxation times is even more limited, with few single field measurements (4–6) and even fewer quantitative magnetic field comparisons available (7). Here we present comprehensive and quantitative measurements of T_1 and T_2 relaxation of water, metabolites, and macromolecules in rat brain under near-identical experimental conditions at three high magnetic field strengths (4.0 T, 9.4 T, and 11.7 T). Besides establishing the contribution of relaxation on sensitivity and resolution, these data will also be valuable for determining optimal image T_1/T_2 contrast, establishing optimal acquisition parameters for quantitative MRS, and determining optimal inversion delays for macromolecule detection or suppression.

MATERIALS AND METHODS

General

All experiments were performed on 1) a 4.0 T Bruker magnet equipped with 15-cm-diameter gradients (128 mT/m in 150 μs; Magnex Scientific, Oxford, UK), 2) a 9.4 T Magnex magnet equipped with 9-cm-diameter gradients (490 mT/m in 175 μs; Resonance Research Inc., Billerica, MA, USA), or 3) a 11.74 T actively-pumped Magnex magnet equipped with 9-cm-diameter gradients (395 mT/m in 120 μs; Magnex Scientific, Oxford, UK). All of the magnets were interfaced to Bruker consoles and operated from Linux computers running Paravision 3.0.1.

RF transmission and signal reception was performed with 14-mm-diameter single-turn surface coils tuned to the proton frequency (170.56, 400.55, and 499.82 MHz at 4.0, 9.4, and 11.74 T, respectively) at each magnetic field.

Animal Preparation

At each magnetic field five male Sprague-Dawley rats (205 ± 22 g, mean ± SD) were prepared in accordance with the guidelines established by the Yale Animal Care and Use Committee. The animals were tracheotomized and ventilated with a mixture of 70% nitrous oxide and 28.5% oxygen under 1.5% halothane anesthesia. A femoral artery was cannulated to monitor blood gases (pO_2, pCO_2), pH, and blood pressure. Physiological variables were maintained within normal limits by small adjustments in ventilation (pCO_2 = 33–45 mm Hg; pO_2 > 120 mm Hg; pH = 7.20–7.38; blood pressure = 90–110 mm Hg). After all surgery was completed, anesthesia was maintained by 0.3–0.8% halothane in combination with 70% nitrous oxide. During NMR experiments the animals were restrained in a head holder, while additional immobilization was obtained with d-tubocurarine chloride (0.5 mg/kg/40 mins, i.p.). The core temperature was measured with a rectal thermosensor and was maintained at 37°C ± 1°C by means of a heated water pad.

MRI Data Acquisition and Processing

Echo-planar imaging (EPI) was performed with an in-house-written PVM method employing a (nonadiabatic)

Magnetic Resonance Research Center, Yale University, School of Medicine, New Haven, Connecticut, USA.

Grant sponsor: NIH; Grant number: R01 EB002097.

*Correspondence to: Robin A. de Graaf, Ph.D., MRRC, Yale University, Departments of Diagnostic Radiology and Biomedical Engineering, TAC, N145, 300 Cedar Street, P.O. Box 208043, New Haven, CT 06520-8043. E-mail: robin.degraaf@yale.edu

Received 11 January 2006; revised 10 March 2006; accepted 6 April 2006.
DOI 10.1002/mrm.20946
Published online 9 June 2006 in Wiley InterScience (www.interscience.wiley.com).

Shinnar-Le Roux (SLR) pulse (pulse length T = 1 or 2 ms, R = bandwidth × pulse length = 5.6) for excitation and two adiabatic full passage (AFP) pulses (hyperbolic secant modulation, T = 2 or 3 ms, R = 10 or 20) for refocusing. Twenty-four axial slices were acquired in an interleaved manner (0.5-mm thickness at 9.4 T and 11.74 T, 0.75-mm thickness at 4.0 T). EPI data acquisition was performed as a data matrix of 128 × 128 over 2.56 × 2.56 cm with eight interleaves and an imaging bandwidth of 200 kHz (9.4 T and 11.7 T) or 100 kHz (4.0 T). The EPI data were processed offline in Matlab 7.0.4. (The Mathworks, Natick, MA, USA) and involved properly combining the interleaved echoes, reversing every other echo, and performing a zero- and first-order phase correction. Image ghosting was typically less than 1% of the maximum signal amplitude. Prior to signal acquisition, the magnetic field homogeneity was optimized by adjusting all first- and second-order shims with an in-house-written version of the FASTMAP method (8) on a centrally-placed 6 × 6 × 6 mm cubic volume, leading to water linewidths of 9.5, 15, and 18 Hz at 4.0, 9.4, and 11.74 T, respectively.

T_1 weighting was introduced by extending the sequence with a nonselective adiabatic half passage (AHP) excitation pulse, a 5000-ms recovery time, and a nonselective AFP inversion pulse. Echo-planar images were acquired at eight variable delays (10, 350, 650, 1000, 1500, 2000, 3000, and 6000 ms) following the inversion pulse. All pixels above a minimum threshold (typically 5% of the maximum signal in the 6000-ms image) were fitted with a three-parameter, single-exponential T_1 recovery function.

T_2 weighting (TR = 3000 ms) was introduced by inserting eight variable delays (30, 35, 40, 45, 50, 60, 75, and 90 ms) symmetrically split around the second AFP refocusing pulse. All pixels above a minimum threshold (typically 5% of the maximum signal in the 30 ms image) were fitted with a two-parameter, single-exponential T_2 decay function.

Tissue regions of interest (ROIs) were manually drawn in Matlab for the corpus callosum, cortex, hippocampus, olfactory bulb, striatum, thalamus, midbrain, and cerebellar gray (GM) and white matter (WM) based on the brain atlas by Paxinos and Watson (9). For all ROIs great care was taken to avoid inclusion of ventricular and cerebrospinal fluid.

MRS Data Acquisition and Processing

Proton MRS was performed with an in-house-written PVM method employing a nonselective AHP excitation pulse (tanh/tan modulation (10), T = 1 ms, R = 150) and three pairs of AFP pulses (sech/tanh modulation, T = 1 or 3 ms, R = 20) for slice-selective refocusing of three orthogonal slices (11). Each AFP pulse was surrounded by 0.5-ms crusher gradients leading to minimum TEs of 12.5 ms at 9.4 T and 11.74 T, and 22.5 ms at 4.0 T. A standard size volume of 5.0 × 3.0 × 5.0 mm ($x \times y \times z$) was selected in the middle of the brain with a dominant contribution from the cerebral cortex (60–70%) and a minor contribution from the corpus callosum and hippocampus. The magnetic field homogeneity was optimized with an in-house-written adiabatic version of the FASTMAP method on a 4 × 4 × 4 cubic volume. Magnetic field homogeneity typically converged within two iterations, leading to water linewidths of 8, 14, and 16 Hz at 4.0, 9.4, and 11.74 T, respectively.

Water suppression was achieved with the adiabatic sequence for water suppression with adiabatic-modulated pulses (SWAMP) method (12) employing either four or six asymmetric AFP pulses ((13) T = 10 ms (9.4 T and 11.74 T) or T = 20 ms (4.0 T)) followed by 1.0 -ms 120 mT/m crusher gradients. Signal was acquired with a 12 ppm spectral bandwidth and a 200–300 ms acquisition time.

T_1 weighting was introduced by extending the MRS sequence with a nonselective AHP excitation pulse, a 5000-ms recovery time, and a nonselective AFP inversion pulse. Signal excitation was executed at 16 variable delays (nonlinearly distributed between 50 and 5000 ms) following the inversion pulse. To minimize effects of motion, frequency drift, and other system instabilities, the inversion delays were employed in random order, and instead of signal averaging each free induction decay (FID) at a given inversion delay 32 times, all 18 × 32 = 576 FIDs were individually stored. Following Fourier transformation and frequency alignment of all spectra, the 576 spectra were separated and summed to yield 18 high-sensitivity, T_1-weighted NMR spectra.

T_1-weighted data sets were acquired at the minimum TE and at TE = 100 ms (9.4 T and 11.75 T) or 125 ms (4 T). In the long-TE data sets, the macromolecular resonances had decayed below the detection limit due to their short-T_2 relaxation time constants (see also Results). At TE = 100 ms the T_1 relaxation of total creatine (creatine + phosphocreatine; CH_2, 3.92 ppm), *myo*-inositol (~ 3.5–3.6 ppm), taurine (3.42 + 3.25 ppm), total choline (~3.2 ppm), total creatine (CH_3, 3.03 ppm), glutamate + glutamine (H4, ~2.3–2.4 ppm) and *N*-acetyl aspartate (NAA; CH_3, 2.01 ppm) were determined. Because of the lower spectral resolution and the specific scalar coupling evolution at TE = 125 ms, T_1 relaxation of *myo*-inositol and taurine could not be determined at 4.0 T. The short-TE data sets were only used to determine the T_1 relaxation of macromolecular resonances M1 (1.7 ppm), M2 (1.4 ppm), M3 (1.1 ppm), and M4 (0.9 ppm).

T_2 weighting (TR = 3000 ms) was introduced by inserting 16 variable delays (nonlinearly distributed between 10 and 450 ms) symmetrically split around the first AFP refocusing pulse. T_2-weighted data sets were acquired and processed as described for T_1-weighted data sets (i.e., random delay order and individually stored FIDs). Since the transverse magnetization of most metabolites is affected by scalar coupling, only the T_2 relaxation of total creatine (CH_2, 3.92 ppm), total choline ($N(CH_3)_3$, ~ 3.2 ppm), total creatine (CH_3, 3.03 ppm), NAA (CH_3, 2.01 ppm), and the macromolecular resonances (M1–M4) were determined.

The NMR spectra were zero-filled to 16 K data points, apodized with an exponential function corresponding to 2 Hz line-broadening, Fourier transformed, and phase corrected (zero-order phase only). Resonance areas were obtained by simple numerical integration following a linear baseline correction. Even at the higher magnetic field strengths, taurine and total choline significantly overlapped at 3.22 ppm. The relaxation parameters for total choline were established by subtracting the taurine resonance intensity at 3.42 ppm from the total integrated intensity of taurine + total choline at 3.22 ppm. Similarly,

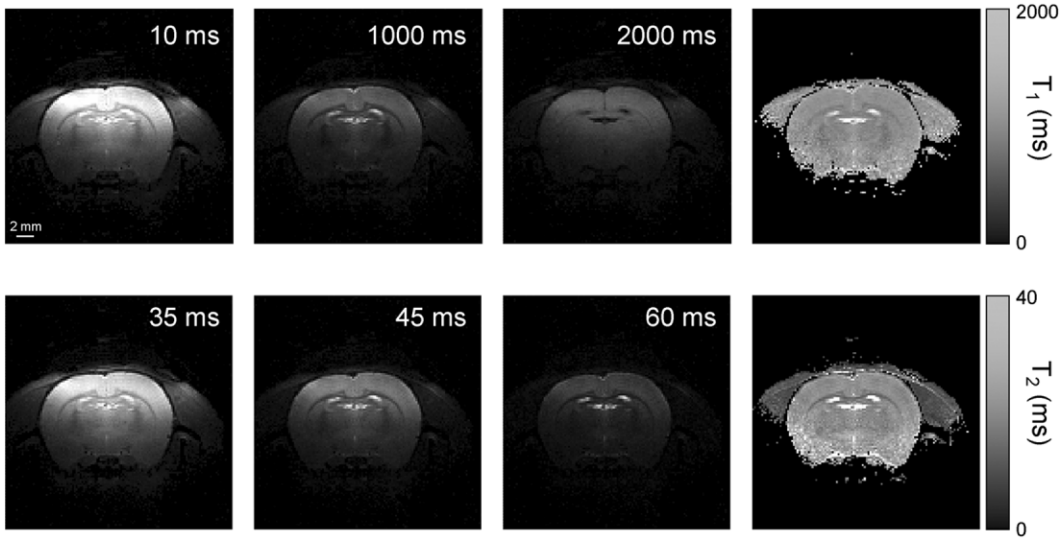

FIG. 1. T_1 (top) and T_2 (bottom) weighted images and calculated maps of rat brain at 9.4 T. The images represent a single 0.5-mm slice extracted from a 24-slice data set. The T_1- and T_2-weighted images show three TIs and TEs, respectively, extracted from eight-TI or -TE data sets. The T_1 and T_2 maps are calculated from three- and two-parameter pixel-by-pixel fits to the T_1- and T_2-weighted data sets, respectively.

lactate and alanine overlapped with macromolecular resonances M2 and M3. To minimize the confounding effects of lactate and alanine on the T_1 measurements, the macromolecular resonances M2 and M3 were considered as one resonance and a 10% signal intensity of lactate and alanine was subtracted assuming an average metabolite T_1 relaxation time constant. The contribution of lactate and alanine on the T_2 measurement was ignored due to complications that arose from the scalar evolution. T_1 and T_2 relaxation curves were fitted with three- and two-parameter, single-exponential functions, respectively.

RESULTS

Figure 1 shows T_1 (top) and T_2 (bottom) weighted images from rat brain at 9.4 T, as well as calculated T_1 and T_2 maps. Because of the surface coil reception profile, the T_1- and T_2-weighted images display a signal decrease with increasing distance from the coil. While the calculated T_1 and T_2 maps appear relatively uniform, the lower signal at distances far away from the surface coil led to an increased error in the calculated T_1 and T_2 relaxation times. The SNR (i.e., the mean image intensity divided by the root mean square noise intensity) in the cortex was 160–170 for T_1 measurements (inversion time (TI) = 5000 ms) and 120–130 for T_2 measurements (TE = 30 ms), respectively. Calculated T_1 and T_2 relaxation times were not included in further data analysis when the SNR of the original T_1- and T_2-weighted images was below 40 and 30, respectively. This roughly corresponds to the inclusion of the upper 7 mm of the brain. Images and maps of similar quality were obtained at 4.0 T and 11.7 T (data not shown).

Figure 2 shows typical ^{1}H NMR spectra acquired from rat brain at 9.4 T. Spectra acquired with long TE (left, TE =

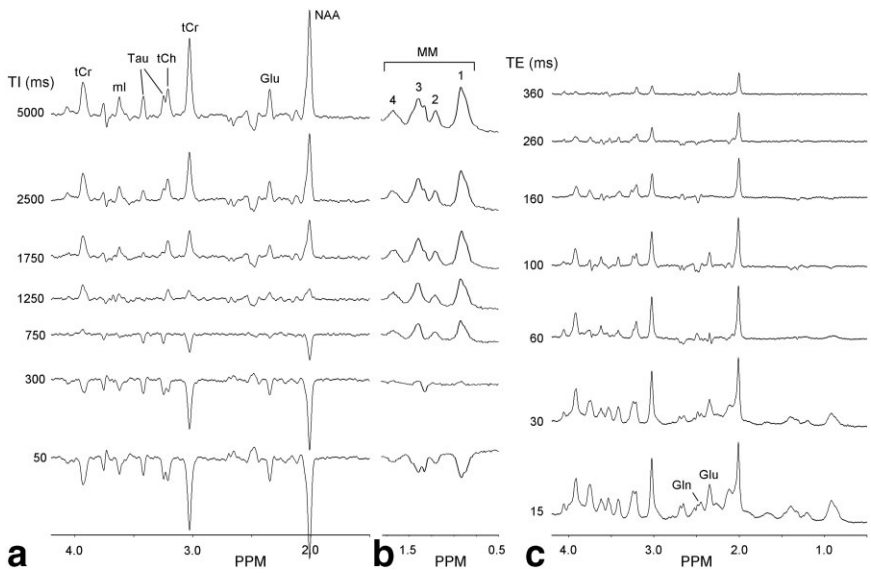

FIG. 2. ^{1}H NMR spectra from rat brain at 9.4 T: T_1-weighted ^{1}H NMR spectra obtained at (**a**) TE = 100 ms and (**b**) TE = 12.5 ms; and (**c**) T_2-weighted ^{1}H NMR spectra. While the integration boundaries are set to include glutamate and glutamine H4 resonances, the great majority of the signal observed at 2.3–2.4 ppm originates from glutamate.

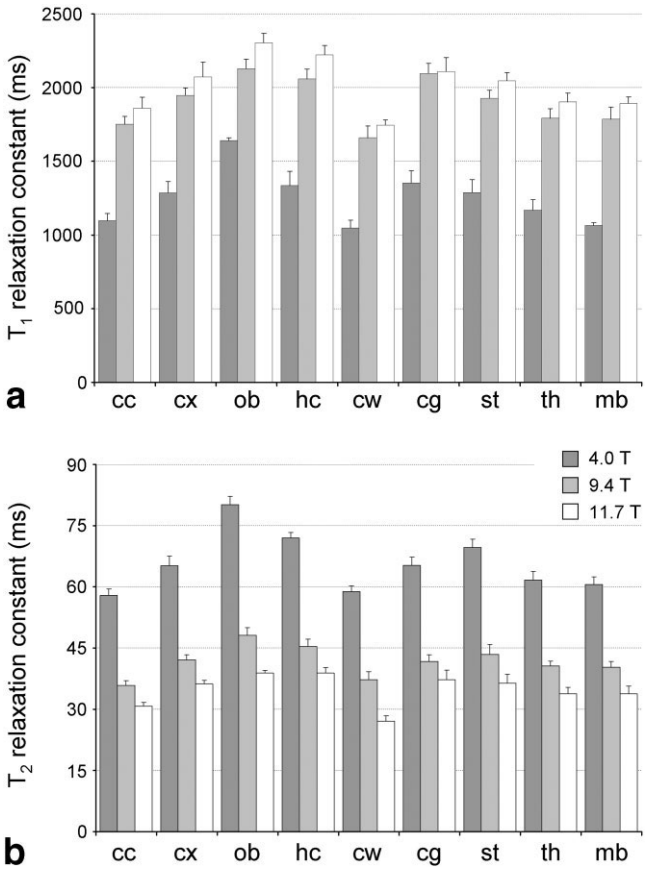

FIG. 3. (**a**) Water longitudinal T_1 relaxation and (**b**) transverse T_2 relaxation in rat brain in vivo at 4.0 T, 9.4 T, and 11.7 T. The analyzed brain structures include the corpus callosum (cc), cerebral cortex (cx), olfactory bulb (ob), hippocampus (hc), cerebellar WM (cw) and GM (cg), striatum (st), thalamus (th), and midbrain (mb). No differentiation was made between different layers in the cortex, hippocampus, or olfactory bulb. Error bars represent the SD over five animals.

100 ms) and short TE (middle, TE = 12.5 ms) during T_1 measurements show excellent SNR, resolution, and stability. The resonances included in further data analysis are indicated as tCr (total creatine), mI (*myo*-inositol), Tau (taurine), tCh (total choline), Glx (glutamate and glutamine), NAA, and MM1–MM4 (macromolecular resonances 1–4). Typical ^{1}H NMR spectra acquired during T_2 measurements are shown on the right. Similar-quality spectra were obtained at 4.0 T and 11.7 T (data not shown).

Figure 3 summarizes the quantitative T_1 and T_2 relaxation times of water in different brain structures at 4.0 T, 9.4 T, and 11.7 T. Without exception, all of the brain structures showed increasing T_1 relaxation constants and decreasing T_2 relaxation constants with increasing magnetic field strength. At all magnetic field strengths the T_1 and T_2 relaxation constants were highest for the olfactory bulb and hippocampus, whereas cerebral (corpus callosum) and cerebellar WM consistently showed the lowest T_1 and T_2 relaxation constants. Table 1 shows the quantitative relaxation constants and standard deviations (SDs).

Figure 4 summarizes the quantitative T_1 and T_2 relaxation times of metabolites and macromolecules at 4 T, 9.4 T, and 11.7 T. While the effect is less than that for water, all metabolites showed a highly significant trend toward higher T_1 and lower T_2 relaxation constants with increasing magnetic field strength. The T_1 relaxation constant of macromolecular resonances increased more rapidly with increasing magnetic field, whereas the macromolecular T_2 relaxation constant was virtually independent of the external magnetic field.

DISCUSSION

Magnetic Field Dependence of T_1 and T_2 Relaxation

Comprehensive and quantitative measurements of water, metabolite, and macromolecule T_1 and T_2 relaxation pa-

Table 1
Water T_1 and T_2 Relaxation Time Constants for Rat Brain at 4.0, 9.4, and 11.7 T

	Structure								
	cc	cx	ob	hc	cw	cg	st	th	mb
4.0 T									
T_1 (ms)	1096.8	1285.8	1640.6	1334.1	1046.9	1352.6	1288.2	1169.4	1064.4
SD (ms)	49.3	77.0	20.8	97.4	53.3	82.6	87.3	69.5	17.3
9.4 T									
T_1 (ms)	1752.1	1948.4	2129.1	2059.7	1660.3	2097.2	1927.0	1793.1	1786.5
SD (ms)	52.1	51.9	63.7	66.1	79.3	68.2	54.7	64.3	81.9
11.7 T									
T_1 (ms)	1861.3	2073.4	2304.3	2222.8	1745.1	2109.4	2046.5	1903.2	1893.2
SD (ms)	73.5	100.7	63.4	63.2	36.0	95.0	55.3	61.2	44.3
4.0 T									
T_2 (ms)	57.9	65.2	80.2	72.0	58.8	65.3	69.7	61.7	60.6
SD (ms)	1.6	2.4	2.0	1.3	1.5	2.0	2.0	2.1	1.9
9.4 T									
T_2 (ms)	35.8	42.1	48.1	45.4	37.2	41.7	43.5	40.6	40.3
SD (ms)	1.2	1.2	1.9	1.8	2.0	1.6	2.4	1.2	1.4
11.7 T									
T_2 (ms)	30.7	36.2	38.9	38.9	27.1	37.3	36.4	33.8	33.8
SD (ms)	1.0	1.0	1.1	1.3	1.3	2.3	2.2	1.6	1.9

cc = corpus callosum, cx = cerebral cortex, ob = olfactory bulb, hc = hippocampus, cw = cerebellar white matter, cg = cerebellar gray matter, st = striatum, th = thalamus, mb = mid-brain.

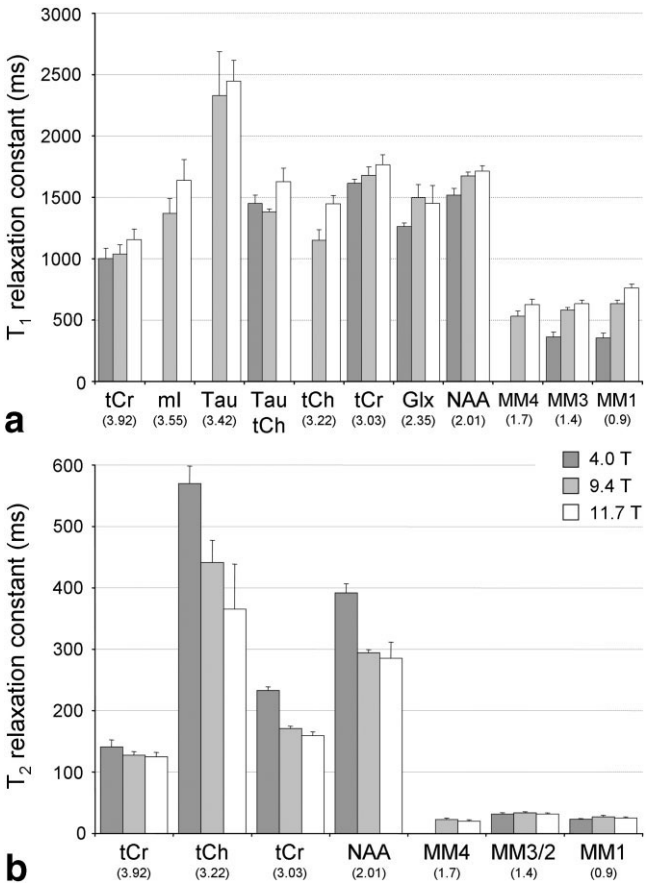

FIG. 4. (**a**) Metabolite and macromolecule longitudinal T_1 relaxation and (**b**) transverse T_2 relaxation in rat brain in vivo at 4.0 T, 9.4 T, and 11.7 T. Metabolite T_1 and T_2 relaxation times were obtained at TE $\geq$ 100 ms to avoid contamination from macromolecular resonances. *Myo*-inositol, taurine, and MM4 could not be reliably determined at 4.0 T with simple integration. Error bars represent the SD over five animals.

rameters at three different magnetic fields has been presented. Since the measurements were performed on similar NMR systems with identical Bruker consoles and comparable RF probes, NMR pulse sequences, and processing, field-dependent variations in T_1 and T_2 relaxation parameters could be observed with high significance.

A primary concern in the early development of high-field NMR was the convergence of T_1 and T_2 relaxation times, which would lead to reduced image T_1/T_2 contrast at higher magnetic fields. In general, T_1 relaxation times increase with increasing field strength, while the absolute differences between tissue T_1's become somewhat smaller. Therefore, overall the T_1 contrast will decrease at higher magnetic fields. However, since the SNR is improved at higher magnetic fields, the CNR is typically higher. This is demonstrated in Fig. 1, where even at 9.4 T and 11.7 T high-quality T_1-weighted images were obtained from rat brain, in close analogy to high-quality T_1-weighted human brain images reported at 7 T (14). Thus T_1-weighting remains a valuable image contrast mechanism even at very high magnetic fields.

Water T_2 relaxation times decreased dramatically at high magnetic fields. However, the relative differences in tissue T_2's remained the same or actually increased with increasing field strength. Therefore, while it may be more difficult to attain the shorter TEs required (especially with EPI), T_2 weighting is a viable high-field image contrast mechanism, as shown by the excellent T_2 contrast obtained at 9.4 T in the rat brain (Fig. 1).

The T_1 relaxation values of water measured at 4.0 T for cerebral GM are in excellent agreement with those published for human brain at 4.0 T (3). However, the measured cerebral WM T_1 values are higher. While intrinsic relaxation differences between human and rat brain cannot be excluded, the observed difference is most likely attributed to partial volume effects in segmenting out the very narrow corpus callosum structure in rat brain. Similar partial volume effects are expected for cerebellar WM T_2 values. However, the T_1 and T_2 differences across the three magnetic fields are still valuable, since the segmentation was performed consistently by a single operator, and the "pure" WM fraction was estimated to be at least 70%. In general, the water T_1 and T_2 relaxation times are in good agreement with published values for water in mouse (15) and rat (16) brain at 7 T.

The increase of water and metabolite T_1 relaxation times with increasing magnetic field strength is in good agreement with the Bloembergen-Purcell-Pound (BPP) theory of dipolar relaxation (17). Based on the long rotation correlation time τ_c of macromolecules, the increasing macromolecular T_1's appear to contradict the BPP theory. However, while τ_c of the overall macromolecule may be long, the rotations of the separate side-chains will be much faster, which makes τ_c much shorter. Furthermore, macromolecular relaxation is likely to be heavily influenced by water T_1 relaxation in the hydration layer surrounding the macromolecule (18).

The sharp decrease of water and metabolite T_2 relaxation times with increasing magnetic field strength is in apparent contradiction to the BBP dipolar relaxation theory, which predicts field-independent T_2 relaxation for a wide range of rotation correlation times. Michaeli et al. (19) explained the field-dependent T_2's as the result of increased dynamic dephasing due to increased local (microscopic) susceptibility gradients. It is well known that both macro- and microscopic magnetic field inhomogeneity due to susceptibility differences between tissues (and air) increases linearly with magnetic field strength. As molecules diffuse through these microscopic field gradients, they lose phase coherence, resulting in a shorter apparent T_2 relaxation time constant, T_2^+. Since diffusion is a random process, the loss in phase coherence cannot be refocused by 180° RF pulses. However, the effect can be minimized during the period between excitation and acquisition by the use of CPMG refocusing, which minimizes the diffusion-weighting and therefore prolongs T_2^+. Unfortunately, because refocusing pulses cannot be applied during signal acquisition, the spectral linewidth will be dominated by T_2^+ relaxation. The large decrease in water T_2 relaxation compared to the almost constant macromolecular T_2 relaxation can also be explained by this in vivo phenomenon since the diffusion coefficient of water ($D \sim 0.7\ \mu m^2/ms$) is more than an order of magnitude larger than that of macromolecules ($D < 0.02\ \mu m^2/ms$) (20). The intermediate diffusion coefficients of metabolites ($D \sim$

Table 2
Metabolite and Macromolecule T_1 and T_2 Relaxation Time Constants for Rat Brain at 4.0, 9.4, and 11.7 T

	Metabolite									
	tCr	mI	Tau	tCh	tCr	Glx	NAA	MM4	MM2,3	MM1
4.0 T										
T_1 (ms)	1003.4			1451.4	1614.0	1262.6	1520.6		360.9	353.5
SD (ms)	81.2			69.1	35.2	28.8	51.3		38.1	38.9
9.4 T										
T_1 (ms)	1039.7	1370.1	2328.9	1348.3	1679.2	1497.5	1674.0	530.6	580.9	632.6
SD (ms)	73.5	120.4	358.6	20.6	67.7	106.5	31.1	42.4	22.1	30.3
11.7 T										
T_1 (ms)	1156.4	1638.1	2447.5	1629.6	1767.3	1450.5	1713.5	627.1	634.1	762.2
SD (ms)	84.5	170.5	167.8	108.7	80.2	146.8	44.1	42.9	25.1	30.4
4.0 T										
T_2 (ms)	140.7			569.8	232.9		391.9		31.7	23.4
SD (ms)	11.5			28.8	5.9		15.1		2.5	1.1
9.4 T										
T_2 (ms)	127.8			441.3	171.1		294.3	22.7	33.5	27.4
SD (ms)	5.7			36.2	3.9		5.1	2.5	1.9	2.3
11.7 T										
T_2 (ms)	124.8			365.7	159.1		285.2	19.9	31.4	25.3
SD (ms)	7.3			73.1	6.6		26.5	2.3	2.1	1.9

0.2 μm^2/ms) are reflected in the intermediate decreases in metabolite T_2 relaxation with increasing magnetic field strength. It should be noted that the observed macromolecular T_2 relaxation times represent a lower boundary, since the TE-dependent signal loss due to scalar coupling evolution was ignored.

Detection of Macromolecular Resonances

Reliable detection of the macromolecular baseline is crucial for quantifying short-TE ^{1}H NMR spectra (6,21). Most commonly the macromolecular baseline is measured with single or double inversion-recovery (IR) sequences (22) based on the difference in longitudinal T_1 relaxation parameters between metabolites and macromolecules. Since the metabolites span a significant range of T_1 relaxation constants, a double-IR (90° – TR – 180° – TI1 – 180° – TI2 – 90° – acquisition) sequence typically gives better metabolite signal suppression than a single-IR (90° – TR – 180° – TI – 90° – acquisition) sequence, at the expense of reduced macromolecular signal recovery. Repetition and inversion delays were determined to give the highest macromolecule-to-metabolite signal intensity ratio over the range of T_1 relaxation times tabulated in Table 2. Table 3 shows the optimized repetition and inversion delays for macromolecule detection at 4.0 T, 9.4 T, and 11.7 T. To avoid excessive experimental measurement times, the TR was set to five times the longest macromolecular T_1 relaxation time. It follows that a single-IR sequence provides a high signal recovery for macromolecular resonances at the expense of a relatively poor suppression of metabolite resonances (as can be judged from the SD on the metabolite signal recovery). Because macromolecular and metabolite T_1 relaxation times converge at higher magnetic fields, the macromolecular signal recovery decreases and the metabolite contamination increases when comparing 4.0 T to 9.4 T and 11.7 T. A double-IR sequence gives much better suppression of metabolite resonances, at the expense of a reduced recovery of macromolecular resonances. Furthermore, a double-IR sequence introduces T_1 weighting into the macromolecular resonances, which becomes more significant at higher magnetic fields (e.g., there is a factor $(57.72 + 9.08)/(57.72 - 9.08) = 1.37$ difference in signal recovery between macromolecular resonances with the lowest and highest T_1 relaxation times at 4.0 T, and this differential signal recovery increases to 1.62 at 11.74 T). While the simplicity of (single or double) IR methods is desirable to establish the macromolecular baseline, the convergence of macromolecular and metabolites T_1's and the resulting differential signal recovery may necessitate more advanced methods, such as the measurement and multiexponential analysis of full T_1 relaxation curves proposed by Hofmann et al. (23).

Table 3
Repetition and Inversion Delays for Macromolecule Detection and Metabolite Suppresion Using (A) Single and (B) Double Inversion Recovery at 4.0, 9.4, and 11.7 T*

	TR[a]	*TI*	S_{MM} (%)[b]	S_{ME} (%)[c]
A				
4 T	2000	850	82.34 ± 6.03	1.48 ± 8.32
9.4 T	3250	1050	67.88 ± 7.37	3.40 ± 11.50
11.7 T	3500	1105	65.97 ± 7.16	3.40 ± 11.63

	TR	*TI*1	*TI*2	S_{MM} (%)[b]	S_{ME} (%)[c]
B					
4 T	2000	1700	540	57.72 ± 9.08	0.37 ± 0.89
9.4 T	3250	2100	630	35.13 ± 8.51	0.35 ± 1.36
11.7 T	3500	2200	660	32.72 ± 7.71	0.49 ± 1.34

*Delays are optimized to achieve the highest $|S_{MM}|S_{ME}|$ ratio for the T_1 values specified in Table 2.
[a]Repetition time *TR* was set to $5T_{1max}(MM)$.
[b]Averaged over 50 linearly-distributed T_1 values in the tabulated *MM* range (Table 2) ± maximum deviation.
[c]Averaged over 50 linearly-distributed T_1 values in the tabulated *ME* range (Table 2) ± standard deviation.

Magnetic Field Dependence of Sensitivity and Resolution

From the presented data, predictions can be made about the magnetic field dependence of SNR and spectral resolution. Ignoring relaxation parameters, the SNR is expected to increase linearly with magnetic field strength B_0 (24). The NMR signal (electromagnetic force (EMF)) induced in a receiving coil increases as the square of B_0 due to two separate and independent factors: First, the spin level population difference increases at higher B_0, and because the energy difference is very small compared to thermal energy, the population increases linearly with B_0, as does the size of the nuclear magnetic dipole moment (i.e., "longitudinal magnetization"). Second, the Larmor frequency at which the magnetic dipole moment precesses is proportional to B_0. Following Faraday's law of electromagnetic induction, the signal produced by a magnetic dipole moment of constant amplitude will increase in proportion (i.e., linearly) to the precession frequency. The combination of these two factors gives a B_0^2 dependence of the signal intensity. However, the noise in high-field NMR experiments will also increase linearly with B_0 (according to the same principles of electromagnetic induction), provided that the subject is the dominant noise source.

Including relaxation, the SNR for a simple, fully-relaxed pulse-acquire experiment can be calculated by considering the amount of signal per unit time (proportional to TR/T_1) acquired over the spectral bandwidth (proportional to $1/(\pi T_2)$, or $1/(\pi T_2^*)$) and is given by

$$SNR \propto B_0 \sqrt{\frac{T_2}{T_1}} \qquad [1]$$

Using the measured T_1 and T_2 relaxation parameters for water and metabolites (Tables 1 and 2), Fig. 5a shows the expected field dependence of the SNR according to Eq. [1]. To obtain values at intermediate fields, the measured T_1 and T_2 relaxation times were modeled to the functions $A[B_0]^B$ and $Aexp(-B_0/B)$, respectively, where A and B were determined by least-squares curve fitting in Matlab. The T_1 function was also used by Bottomley et al. (1) for water and can adequately fit T_1 relaxation data over the range of 0–500 MHz. It follows that the SNR for singlet resonances in NMR spectroscopy increases less than linearly with B_0, while the SNR for water starts to level off for magnetic fields beyond 7 T, and may even show a maximum at around 20 T. It should be noted that while the SNR of metabolites increases less than linearly with B_0, the quantification accuracy of metabolites (and especially lower-concentration, scalar-coupled metabolites) may increase much better than linearly with B_0 due to reduced spectral overlap and simplified spectral patterns.

Besides increased SNR and decreased strong coupling effects, the main advantage of high magnetic fields for MRS is the increased spectral dispersion and spectral resolution. The spectral linewidth $\Delta\nu$ of a single resonance can be described by

$$\Delta\nu = \frac{1}{\pi T_2^*} = \frac{1}{\pi T_2^\dagger} + \gamma \Delta B_0 \qquad [2]$$

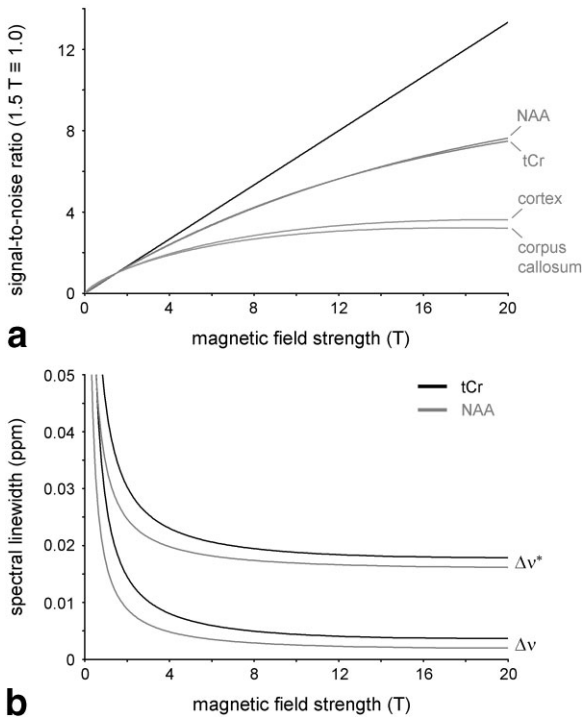

FIG. 5. Calculated magnetic field dependence of (**a**) SNR and (**b**) spectral resolution extrapolated from measured data at 4.0 T, 9.4 T, and 11.7 T (dotted lines)

where ΔB_0 represents the residual macroscopic magnetic field inhomogeneities, and $T_2^\dagger$ represents the apparent T_2 relaxation time as discussed above. With use of a constant, second-order shimming technique (FASTMAP) at all magnetic fields, the residual magnetic field inhomogeneities are expected to scale linearly with B_0. Additional line-broadening due to B_0 inhomogeneities were measured from the total creatine, NAA, and water resonances, and averaged out as 2.6 Hz, 5.8 Hz, and 7.2 Hz at 4.0 T, 9.4 T, and 11.7 T, respectively. Using Eq. [2], the estimates for $\gamma\Delta B_0$ and the T_2 relaxation times summarized in Table 2 allow a prediction for the field dependence of the spectral linewidth ($\Delta\nu/B_0$), as shown in Fig. 5b. It follows that the spectral linewidth converges to ~0.015–0.020 ppm for $B_0 > 9.4$ T. The spectral linewidth at low magnetic fields ($B_0 < 2$ T) is relatively broad because at those fields the inherent T_2 relaxation dominates the linewidth. Only at $B_0 > 9.4$ T do the magnetic field inhomogeneities become the dominant contribution to the observed spectral linewidth. Based on the curves in Fig. 5b, it is not expected that the spectral resolution for single resonances will dramatically increase beyond $B_0 \sim 9.4$ T. However, significant improvements in spectral resolution for scalar-coupled spin-systems, such as glutamate and glutamine, is expected well beyond 9.4 T. Note that the inherent spectral linewidth (based on T_2) converges to 0.005 ppm (and ultimately to 0 ppm). Therefore, significant improvements can be expected when MR spectra based on T_2 alone can be acquired (25). Possible strategies to accomplish this goal may be found in 2D NMR approaches in combination with CPMG signal refocusing, as suggested by Michaeli et al. (19).

CONCLUSIONS

In vivo NMR has seen a steady drive toward higher magnetic fields, in part because such fields intrinsically provide better sensitivity and resolution, and in part for application-specific reasons, such as improved spatial specificity in BOLD fMRI (e.g., Refs. 14 and 26, and references therein). However, conducting experiments at high magnetic field strengths entails high monetary costs, requires expertise in RF coil design, and involves a substantial list of potential complications, including increased B_0 and B_1 magnetic field inhomogeneities (27), RF power deposition, and acoustic noise generation. A thorough understanding of the relative gains is therefore crucial for making a balanced decision regarding the use of higher magnetic fields. The data presented here provide a partial insight into several aspects of high-field in vivo NMR. The longest-standing argument for using high-field in vivo NMR (i.e., its increased sensitivity) becomes less dominant as T_1 and T_2 relaxation constants increase and decrease, respectively. Therefore, T_1/T_2-based anatomical imaging and even diffusion tensor imaging (DTI) do not necessarily have to be performed at the absolute highest magnetic field strength. If sensitivity is the primary concern, the implementation of phased-array receiver RF coils (28) or cooled/superconducting RF coils (29,30) can under certain conditions increase the sensitivity much faster (and with less expense) than an increase in magnetic field strength, and circumvent the complications of high-field NMR.

For fMRI, and in particular BOLD fMRI, the situation is distinctly different. The BOLD effect scales linearly with magnetic field strength (31,32) and, more importantly, the BOLD effect becomes spatially more specific because the contribution of nonspecific draining vein effects becomes negligible at 7 T or higher (33,34). Therefore, despite the complications of increased B_0 magnetic field inhomogeneities, it is desirable to perform BOLD fMRI studies of functional brain activation at the highest magnetic field.

For NMR spectroscopy a higher magnetic field strength is always desirable. The spectral resolution of singlet resonances continues to improve up to ~9.4 T, while the quantification accuracy of strongly-coupled and low-concentration metabolites will continue to improve well beyond 9.4 T. Therefore, both the information content and the quantification accuracy of metabolites will improve at higher magnetic fields, as will be experimentally demonstrated in a subsequent paper on field-dependent metabolite quantification. However, the majority of (clinical) NMR spectroscopy studies only detect and quantify the singlet resonances of total choline, total creatine, and NAA at longer TEs. Since these resonances are well separated even at 1.5 T, the arguments for higher magnetic fields are less strong when the detection is limited to these three resonances. However, the improved SNR at higher magnetic fields can of course always be used to detect the singlet resonances from smaller volumes.

High-magnetic-field systems in the major MR centers worldwide have generated impressive new insights into brain structure, function, and metabolism by combinations of fMRI and NMR spectroscopy and continuing improvements in hardware. While the advantages of high-field NMR should always be a prime consideration, it is hoped that the data and arguments presented here can be used to guide the experimentalist in optimal sequence design (e.g., TR/TE) at a given magnetic field strength.

ACKNOWLEDGMENT

The authors thank Bei Wang for expert animal preparation.

REFERENCES

1. Bottomley PA, Foster TH, Argersinger RE, Pfeifer LM. A review of normal tissue hydrogen NMR relaxation times and relaxation mechanisms from 1–100 MHz: dependence on tissue type, NMR frequency, temperature, species, excision, and age. Med Phys 1984;11:425–448.
2. Kim SG, Hu X, Ugurbil K. Accurate T1 determination from inversion recovery images: application to human brain at 4 Tesla. Magn Reson Med 1994;31:445–449.
3. Hetherington HP, Pan JW, Mason GF, Adams D, Vaughn MJ, Twieg DB, Pohost GM. Quantitative ^{1}H spectroscopic imaging of human brain at 4.1 T using image segmentation. Magn Reson Med 1996;36:21–29.
4. Frahm J, Bruhn H, Gyngell ML, Merboldt KD, Hanicke W, Sauter R. Localized proton NMR spectroscopy in different regions of the human brain in vivo. Relaxation times and concentrations of cerebral metabolites. Magn Reson Med 1989;11:47–63.
5. van der Toorn A, Dijkhuizen RM, Tulleken CA, Nicolay K. T1 and T2 relaxation times of the major ^{1}H-containing metabolites in rat brain after focal ischemia. NMR Biomed 1995;8:245–252.
6. Pfeuffer J, Tkac I, Provencher SW, Gruetter R. Toward an in vivo neurochemical profile: quantification of 18 metabolites in short-echo-time ^{1}H NMR spectra of the rat brain. J Magn Reson 1999;141:104–120.
7. Ethofer T, Mader I, Seeger U, Helms G, Erb M, Grodd W, Ludolph A, Klose U. Comparison of longitudinal metabolite relaxation times in different regions of the human brain at 1.5 and 3 Tesla. Magn Reson Med 2003;50:1296–1301.
8. Gruetter R. Automatic, localized in vivo adjustment of all first- and second-order shim coils. Magn Reson Med 1993;29:804–811.
9. Paxinos G, Watson C. The rat brain in stereotaxic coordinates. New York: Academic Press; 1997.
10. Garwood M, Ke Y. Symmetric pulses to induce arbitrary flip angles with compensation for RF inhomogeneity and resonance offsets. J Magn Reson 1991;94:511–525.
11. Garwood M, DelaBarre L. The return of the frequency sweep: designing adiabatic pulses for contemporary NMR. J Magn Reson 2001;153:155–177.
12. de Graaf RA, Nicolay K. Adiabatic water suppression using frequency selective excitation. Magn Reson Med 1998;40:690–696.
13. Hwang TL, van Zijl PC, Garwood M. Asymmetric adiabatic pulses for NH selection. J Magn Reson 1999;138:173–177.
14. Ugurbil K, Adriany G, Andersen P, Chen W, Garwood M, Gruetter R, Henry PG, Kim SG, Lieu H, Tkac I, Vaughan T, Van De Moortele PF, Yacoub E, Zhu XH. Ultrahigh field magnetic resonance imaging and spectroscopy. Magn Reson Imaging 2003;21:1263–1281.
15. Guilfoyle DN, Dyakin VV, O'Shea J, Pell GS, Helpern JA. Quantitative measurements of proton spin-lattice T_1 and spin-spin T_2 relaxation times in the mouse brain at 7.0 T. Magn Reson Med 2003;49:576–580.
16. Cremillieux Y, Ding S, Dunn JF. High-resolution in vivo measurements of transverse relaxation times in rats at 7 Tesla. Magn Reson Med 1998;39:285–290.
17. Bloembergen N, Purcell EM, Pound RV. Relaxation effects in nuclear magnetic resonance absorption. Phys Rev 1948;73:679–712.
18. Zhong JH, Gore JC, Armitage IM. Quantitative studies of hydrodynamic effects and cross-relaxation in protein solutions and tissues with proton and deuteron longitudinal relaxation times. Magn Reson Med 1990; 13:192–203.
19. Michaeli S, Garwood M, Zhu XH, DelaBarre L, Andersen P, Adriany G, Merkle H, Ugurbil K, Chen W. Proton T_2 relaxation study of water, *N*-acetylaspartate, and creatine in human brain using Hahn and Carr-Purcell spin echoes at 4T and 7T. Magn Reson Med 2002;47:629–633.
20. Pfeuffer J, Tkac I, Gruetter R. Extracellular-intracellular distribution of glucose and lactate in the rat brain assessed noninvasively by diffusion-weighted 1H nuclear magnetic resonance spectroscopy in vivo. J Cereb Blood Flow Metab 2000;20:736–746.
21. Behar KL, Ogino T. Characterization of macromolecule resonances in the ^{1}H NMR spectrum of rat brain. Magn Reson Med 1993;30:38–44.

22. Hwang JH, Graham GD, Behar KL, Alger JR, Prichard JW, Rothman DL. Short echo time proton magnetic resonance spectroscopic imaging of macromolecule and metabolite signal intensities in the human brain. Magn Reson Med 1996;35:633–639.
23. Hofmann L, Slotboom J, Boesch C, Kreis R. Characterization of the macromolecule baseline in localized ^{1}H-MR spectra of human brain. Magn Reson Med 2001;46:855–863.
24. Redpath TW. Signal-to-noise ratio in MRI. Br J Radiol 1998;71:704–707.
25. Behar KL, Ogino T. Assignment of resonance in the 1H spectrum of rat brain by two-dimensional shift correlated and J-resolved NMR spectroscopy. Magn Reson Med 1991;17:285–303.
26. Chen W, Ugurbil K. High spatial resolution functional magnetic resonance imaging at very-high-magnetic field. Top Magn Reson Imaging 1999;10:63–78.
27. Vaughan JT, Garwood M, Collins CM, Liu W, DelaBarre L, Adriany G, Andersen P, Merkle H, Goebel R, Smith MB, Ugurbil K. 7T vs. 4T: RF power, homogeneity, and signal-to-noise comparison in head images. Magn Reson Med 2001;46:24–30.
28. Roemer PB, Edelstein WA, Hayes CE, Souza SP, Mueller OM. The NMR phased array. Magn Reson Med 1990;16:192–225.
29. Wright AC, Song HK, Wehrli FW. In vivo MR micro imaging with conventional radiofrequency coils cooled to 77 degrees K. Magn Reson Med 2000;43:163–169.
30. Black RD, Early TA, Roemer PB, Mueller OM, Mogro-Campero A, Turner LG, Johnson GA. A high-temperature superconducting receiver for nuclear magnetic resonance microscopy. Science 1993;259:793–795.
31. Ogawa S, Lee TM, Kay AR, Tank DW. Brain magnetic resonance imaging with contrast dependent on blood oxygenation. Proc Natl Acad Sci USA 1990;87:9868–9872.
32. Gati JS, Menon RS, Ugurbil K, Rutt BK. Experimental determination of the BOLD field strength dependence in vessels and tissue. Magn Reson Med 1997;38:296–302.
33. Lee SP, Silva AC, Ugurbil K, Kim SG. Diffusion-weighted spin-echo fMRI at 9.4 T: microvascular/tissue contribution to BOLD signal changes. Magn Reson Med 1999;42:919–928.
34. Duong TQ, Yacoub E, Adriany G, Hu X, Ugurbil K, Kim SG. Microvascular BOLD contribution at 4 and 7 T in the human brain: gradient-echo and spin-echo fMRI with suppression of blood effects. Magn Reson Med 2003;49:1019–1027.